

# Macroscopic Orientational Gold Nanorods Monolayer Film with Excellent Photothermal Anticounterfeiting Performance

Liping Song, Nianxiang Qiu, Youju Huang,\* Qian Cheng, Yanping Yang, Han Lin, Fengmei Su, and Tao Chen\*

Constructing 2D gold nanorods monolayer films with precise particle assembly is of great importance to fundamental and real applications. However, it is usually difficult to achieve macroscopic size, freestanding feature, high density of particle packing, and precisely controllable particle orientation in monolayer films. In this work, a macroscopic, uniform, freestanding orientational monolayer film is facilely and controllably prepared through precise assembly of asymmetrically modified gold nanorods at water–oil interface. The assembling morphologies can be controlled through regulating the interaction between gold nanorods by varying the amounts and sites of modified molecules. The intriguing tunable assemblies exhibit not only adjustable absorption spectrum in a wide range attributed to different particle coupling, but also optimized photothermal conversion capability under low energy density ( $0.08 \text{ W cm}^{-2}$ ). Together with a commercial thermochromic dye, the patterned assemblies show excellent photothermal anti-counterfeiting performance by reproducing accurate full images in 20 s that are invisible after laser off in 10 min. The excellent laser writing performance is also demonstrated by writing any information on thermochromic dye-coated assemblies. With the advantages of being macroscopic, equipment-free, transferable, scalable and with high photothermal conversion capability, the orientational monolayer films pave the way for on-demand design of sensing and device applications.

arrangement will potentially facilitate the development of sensing and further benefit the manufacture of optoelectronic and healthcare devices.<sup>[1–6]</sup> Technologies for manipulating assembling behaviors of Au NPs, especially anisotropic Au NPs (e.g., Au NRs), are widely exploited.<sup>[7–9]</sup> Generally, there are two main methods to assemble Au NPs into designed arrangement: solution assembly and interfacial assembly. As a fact, a great deal of in-depth progress has been made in manipulating Au NPs assemblies in solution and abundant assembling strategies have been developed.<sup>[10–12]</sup> Because of the designable molecular interaction and remarkable spectral shift of assemblies attributed to the tunable particle spacing, the sensing and detection applications of assembling Au NPs in solution are significantly inspired.<sup>[7,13,14]</sup> Extensive investigations have focused on the structural optimization of Au NPs assemblies in solution, but there are two main roadblocks that hindered its practical applications. First, the formation of Au NPs assemblies often relies on strict solvent

environment and modified molecular conditions.<sup>[15,16]</sup> In addition, the poor stability and finite assembly amounts are difficult to overcome, which will limit its practical applications in devices.<sup>[17]</sup>

## 1. Introduction

Organizing gold nanoparticles (Au NPs) into uniform assemblies with controllable particle spacing and particle


L. Song, Dr. N. Qiu, Prof. Y. Huang, Q. Cheng, Y. Yang, Prof. T. Chen  
Key Laboratory of Marine Materials and Related Technologies  
Zhejiang Key Laboratory of Marine Materials and Protective  
Technologies  
Ningbo Institute of Material Technology and Engineering  
Chinese Academy of Sciences  
Ningbo 315201, China

E-mail: yjhuang@hznu.edu.cn; tao.chen@nimte.ac.cn

L. Song, Dr. N. Qiu, Q. Cheng, Y. Yang, Prof. T. Chen  
School of Chemical Sciences  
University of Chinese Academy of Sciences  
Beijing 100049, China

Prof. Y. Huang, H. Lin  
College of Materials, Chemistry and Chemical Engineering  
Hangzhou Normal University  
Hangzhou 311121, China

Dr. F. Su  
National Engineering Research Centre for Advanced Polymer  
Processing Technology  
Key Laboratory of Materials Processing and Mold  
(Zhengzhou University)  
Ministry of Education  
Zhengzhou University  
Zhengzhou 450002, China

 The ORCID identification number(s) for the author(s) of this article can be found under <https://doi.org/10.1002/adom.201902082>.

DOI: 10.1002/adom.201902082

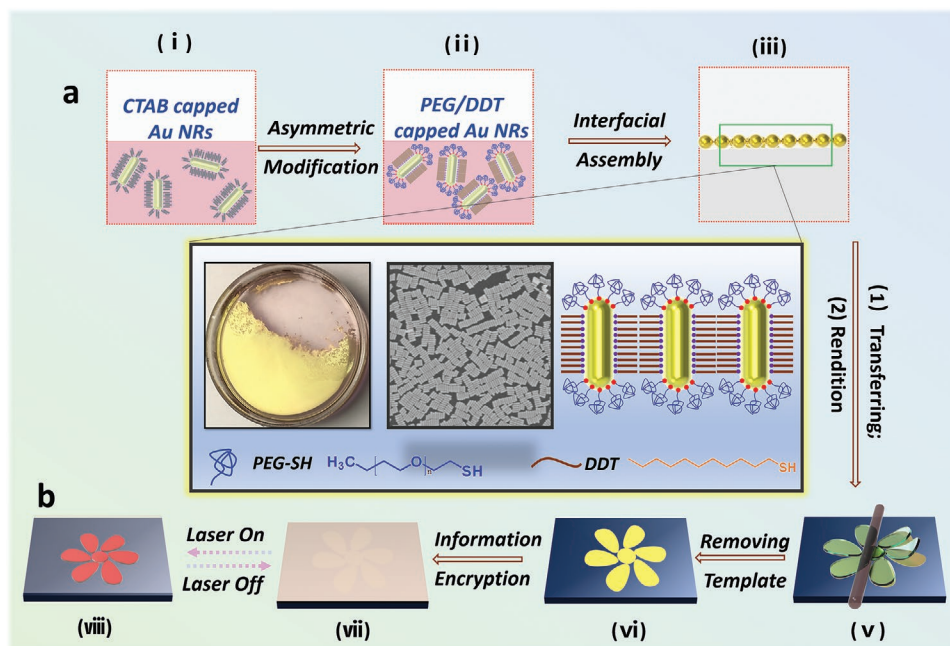


**Figure 1.** Schematic illustration of a) the preparation process of macroscopic assemblies and b) the application of aligned Au NRs arrays in photo-thermal anticounterfeiting.

The macroscopic assembling size and high stability of Au NPs assemblies engenders distinctive superiorities of interfacial assembly.<sup>[18]</sup> Various approaches have been explored to optimize the properties of interfacial assemblies.<sup>[19–21]</sup> Among them, water–oil interfacial assembly attracts much more attention, due to high accessibility, operability, macroscopic assembling areas, and controllable interparticle distances.<sup>[22–25]</sup> However, achieving uniform and macroscopic Au NPs monolayer with controllable particle spacing and arrangement is much more challenging.<sup>[26]</sup> In addition, the availability of particles to assemblies was also limited. For instance, sodium-citrate-coated Au NPs were relatively difficult to assemble into films compared to cetyltrimethylammonium bromide (CTAB)-coated ones by utilizing ethanol promoted oil–water interfacial assembling.<sup>[22]</sup> Additionally, it is usually strictly affected by slight interference (temperature, pH, pressure). In our recent works, we have succeeded in constructing macroscopic Au NPs monolayer films with closely packed nanoparticles and controllable reversibly plasmonic properties.<sup>[27,28]</sup> Unfortunately, there are still no effective ways to achieve macroscopic orientational assembling structures of anisotropic Au NPs (gold nanorods, Au NRs), which strongly hindered the LSPR dependent optical applications.<sup>[29–32]</sup>

Here, we demonstrate a controllable Au NRs assembling structure with macroscopic size, orientational particle arrangement, and adjustable adsorption via combining precise asymmetric modification of gold particles with water–oil interfacial assembly. Au NRs were precisely asymmetric modified with mercapto-polyethylene glycol (PEG-SH) and hydrophobic sulfhydryl molecule (1-dodecanethiol, DDT) according to Murray's theoretical calculation,<sup>[33–35]</sup> illustrated schematically in **Figure 1**. Then, the aligned Au NRs assemblies were obtained by utilizing the reported water–oil interfacial

methods.<sup>[22]</sup> As a hydrophilic sulfhydryl molecule with large molecular weight, PEG-SH plays a key role in the orientational assembly process of Au NRs. Thus, the amounts of PEG-SH were adjusted to optimize the assembling structure. Molecular dynamics simulations are utilized to elucidate the role of the main molecules in the assembling system, and we thus proposed an assembly mechanism. Furthermore, the controllable UV adsorption from the macroscopic orientational Au NRs arrays makes this system extremely attractive and match the light source to reach optimum photothermal conversion, as demonstrated by previous similar works.<sup>[36]</sup> Under low laser energy density, the Au NRs side by side (SS) assembly shows high and rapid photothermal response. With the assistance of thermochromic dyes, photothermal anticounterfeiting performance of different patterns and writing performance of Au NRs SS assembly were investigated. This work provides a facile method for the preparation of macroscopic aligned Au NRs arrays, which is promising in enhancing the performance of anticounterfeiting devices.

## 2. Result and Discussion

Au NRs with the aspect ratio of 3.5 were prepared according to the well-known seeded growth method (Figure S1, Supporting Information).<sup>[37]</sup> It is noteworthy that Au NRs with aspect ratios higher than 3.5 were probably formed spontaneously into the orientational assemblies under the assistance of CTAB.<sup>[38–40]</sup> There are several differences between our approach and the previous work. The previous assembly based on CTAB interaction is conducted on solid substrate and the assembly area is limited. It is very easy to obtain macroscopic and uniform assemblies via our present interfacial assembly approach.

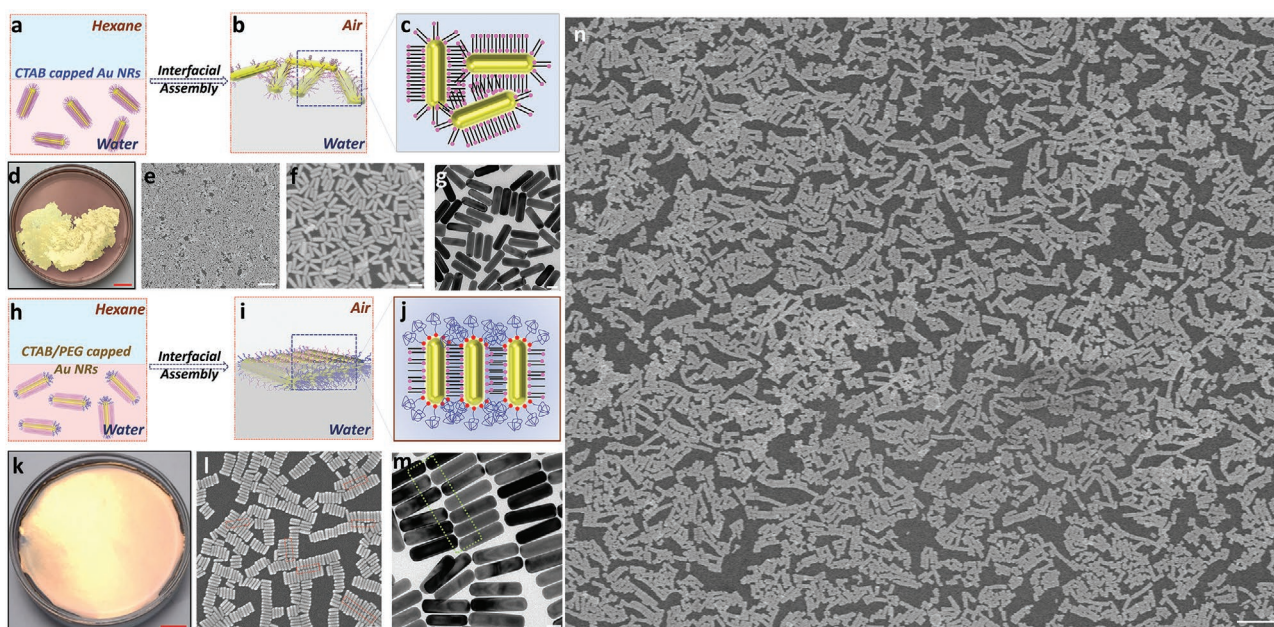


**Figure 2.** The a,b) assembling and c) molecules interacting schematic diagram, d) the corresponding photograph, e,f) SEM images and g) TEM image of Au NRs assemblies without asymmetric modification. Au NRs SS assemblies with precisely asymmetric modification: ends of Au NRs modified with PEG-SH completely and sides of Au NRs with CTAB: h,i) The assembling and j) molecules interacting schematic diagram, k) the corresponding photograph, l) SEM image, m) TEM image, and n) SEM images of macroscopic aligned Au NRs assemblies. The scale bars in (d,k) are 1 cm; the scale bars in (e,n) are 1  $\mu\text{m}$ ; the scale bars in (f,l) are 100 nm; the scale bars in (g,m) are 50 nm.

In addition, the assembly via spontaneous CTAB interaction still has some problems: 1) It is not universal. As mentioned, only with larger aspect ratios, it is feasible for constructing Au NRs SS assembling structures. However, the aspect ratio of Au NRs that are usually prepared is about 3–4. 2) the interaction mode between CTAB molecules is sophisticated. In addition, the CTAB on ends of Au NRs would interfere with SS assembly of Au NRs. 3) CTAB possess fluxility on the surface of Au NRs that is easy to make the assembly system unstable. 4) CTAB is the structure directing agent and stabilizer in the process of Au NRs synthesis. Thus, it is difficult to precise quantification of CTAB on Au NRs. Therefore, in this work, the Au NRs with small aspect ratio were chosen to efficiently exclude the possible effect. The water–oil interfacial assembly have been an efficient approach to obtain macroscopic Au NPs assemblies.<sup>[22,41,42]</sup> Thus, it is of great importance to identify the detailed assembly mechanism. Briefly, as shown in Figure S2, Supporting Information, a certain amount of hexane was added to the surface of Au NRs aqueous dispersions, and then a small amount of ethanol was slowly injected to water phase. The process of ethanol injection was accompanied with the evaporation of hexane and Au NRs assembled at water/hexane interface.<sup>[22,43,44]</sup> After the complete ethanol injection, the golden film was clearly visible. Generally, the assembling system contains oil/water two-phase, and the organic phase (e.g., hexane) must meet three basic conditions: easy to volatile, low density, and insoluble with water.<sup>[43,45,46]</sup> It is known to all that surfactant on the surface of gold nanoparticles makes them dispersible uniformly in water phase and the contact angle ( $\theta$ ) of them is lower than  $90^\circ$ .<sup>[46,47]</sup> Nevertheless, on the addition of another low-dielectric solvent (alcohol) to the water phase,

the stability of gold nanoparticles can be destroyed, resulting in their contact angle approaching  $90^\circ$ ,<sup>[48,49]</sup> and spontaneous particles moving to the water/oil interface, due to the reduce of the interface energy.<sup>[50,51]</sup>

Conventionally, CTAB-capped Au NRs were assembled into 2D films in large area via water–oil interfacial assembly (Figure 2a–g). It is clear that Au NRs are randomly packed in the film, including multiple assembling morphologies such as side by side (SS), end to end (EE), and end to side (ES) (Figure 2g). It is well known that CATB-capped Au NRs in solution show steric or electrostatic repulsion due to the positive CTAB.<sup>[52,53]</sup> However, many investigations have shown that CTAB molecules presented promoting effects with concentrating Au NRs solution via strong van der Waals (vdW) forces.<sup>[38–40]</sup> Therefore, the Au NRs forming multiple assembling morphologies were expected from the interaction between CTAB molecules (Figure 2a–c). As shown in Figure S3, Supporting Information, four assembly modes were revealed according to the interaction manner (sharing a common layer of counterions or interdigitating of CTAB tails from neighboring NPs) of CTAB.<sup>[54]</sup> Statistically, most Au NRs presented a disorderly arrangement while SS assemblies held 30%. CTAB-coated Au NRs always presented an SS assembly according to the Hamaker integral approximation about the vdW potentials<sup>[13,39]</sup>:

$$U_{\text{SS}} = -\frac{Aha^{1/2}}{24L^{3/2}} \quad (1)$$

$$U_{\text{EE}} = -\frac{Aa^2}{12L^2} \quad (2)$$

Here,  $h$  and  $a$  represent the length and radius of Au NRs, respectively;  $L$  is the interparticle distance between two particle centers;  $A$  is the Hamaker coefficient that is estimated to be  $A = 5 \times 10^{-20}$  J (or 13 kT at room temperature)<sup>[55]</sup> in which the value of  $U_{SS}/U_{EE}$  ( $hL^{1/2}/2a^{3/2}$ ) is slightly larger than unity. However, the assemblies of CTAB-coated Au NRs was not uniform (Figure 2d,e). It is worth noting that there is really no exact standard for the number of Au NRs as for the standard of EE/SS. For example, the head-to-head arrangement of two or more Au NRs is considered as EE assembly in some reported works.<sup>[56–58]</sup> And as for the SS assembly, the shoulder-to-shoulder arrangement of three or more Au NRs is also considered.<sup>[59,60]</sup> Therefore, the assembly mode of Au NRs is not determined by the number of Au NRs in the assembly. Rather, it depends on the proportion of such oriented (EE/SS) assemblies in the overall assembly. In this work, the SS or EE assemblies were distinguished according to the holistic orientation.

The assembly state can be attributed to the following reasons: In the process of Au NRs assembly, close Au NRs are close to each other promoted by the molecular interaction on the surface to form SS assemblies containing several or more Au NRs.

In order to precisely control the Au NRs assembling morphology, the regulation of surface chemistry and interaction of Au NRs would be a possible way. As we have known, the sulfhydryl molecule would be preferentially attached to the end region of Au NRs via the function of Au-S bonding,<sup>[16,61]</sup> due to homogeneous distributed CTAB on Au NRs and the higher curvature of the end parts (100 face).<sup>[16,62,63]</sup> Accordingly, the asymmetric modification was acquired by critical calculation, as shown in Figure S4, Supporting Information, and Section 4.<sup>[35,60,64]</sup> Based on the mature technology of asymmetric modification of Au NRs, the commonly used sulfhydryl molecule (PEG-SH) was induced to synergistically tailor Au NRs. As shown in Figure 2h–j, Au NRs were modified with a

certain amount of PEG-SH (slightly larger than the calculated end modification amounts). Apparently, the macroscopic and uniform golden films were visible, and the assembly area was as large as 40 cm<sup>2</sup> that was never achieved in previous work<sup>[22,27]</sup> (Figure 2k). In addition, the asymmetrically modified Au NRs presented macroscopic SS assembly structures with an orientation rate approaching 100% (Figure 2l–n).

It is known to all that the sulfhydryl molecule presented as random coils were easily entangled together.<sup>[35]</sup> In addition, our previous work have verified that the affinity between PEG molecule could regulate the directional assembly of Au NRs.<sup>[21]</sup> The experimental results showed that almost all SS assemblies showed intimate contact with neighboring ones (marked in Figure 2l,m). In the interfacial assembly process, Au NRs assembly were affected by many factors, including intermolecular forces on the surface of Au NRs, solvation, air pressure, and temperature. Therefore, there is still no way to obtain the ideal fully aligned dense assembly structure of Au NRs (except, of course, the top-down approach). Thus, we inferred that two forces synergistically promote the directional SS assembly of Au NRs: the van der Waals forces between CTAB on sides of Au NRs and the molecular entanglement between PEG on ends of Au NRs. The inhomogeneous and multiple van der Waals forces between CTAB made the Au NRs SS assemblies present inconsistent interparticle gaps (marked in Figure 2m). However, the ethanol-induced water–oil interface assembly process is rapid and Au NRs reached the stable state before they are all arranged in a certain orientation. These results proved that the PEG-SH selectively capped on the end regions of Au NRs would prefer the formation of Au NRs SS structures.

To further clarify the directional assembly of Au NRs in film, different amounts of PEG-SH were used for selectively modify Au NRs. As shown in Figure 3, without PEG-SH added to the system, Au NRs presented a disordered arrangement (Figure 3a). On increasing the amount of PEG-SH, SS assemblies clearly

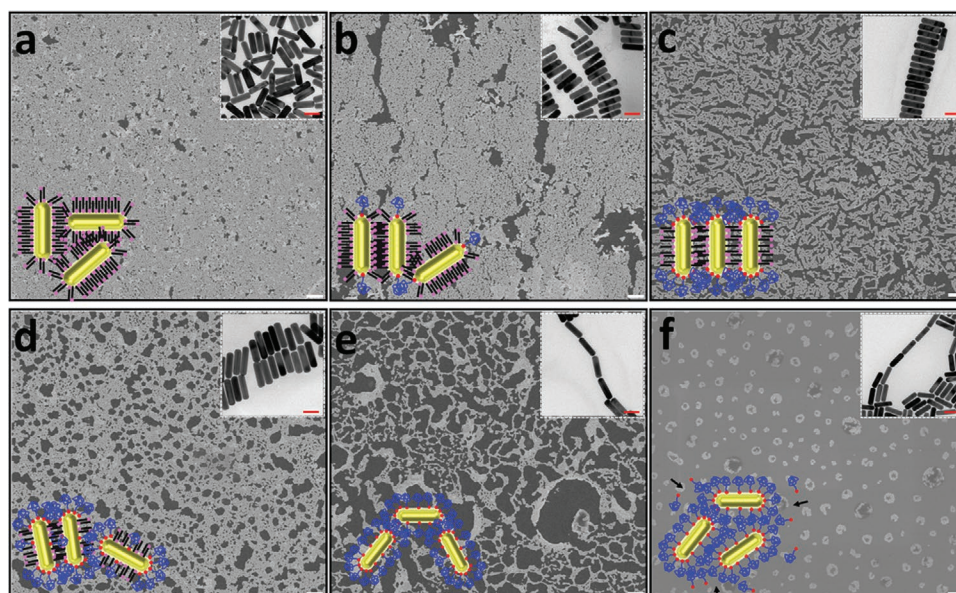


**Figure 3.** The SEM and TEM images of Au NRs monolayers by modifying Au NRs with different amount of PEG-SH (10 mM) (a–f: 0  $\mu$ L, 3  $\mu$ L, 7  $\mu$ L, 10  $\mu$ L, 20  $\mu$ L, 50  $\mu$ L). The concentration of Au NRs and PEG-SH aqueous solution are 7.89 mM and 1 mM, respectively. The scale bar is 1  $\mu$ m, and the inset scale bar is 100 nm.

appeared (Figure 3b). However, the length of SS assemblies was short and some Au NRs were still disordered. The end regions of Au NRs were completely capped and extremely orderly SS assemblies were present with increasing amount of PEG-SH (Figure 3c). It is very important to point out that the SS assemblies were large-scaled and the orientation ratio was almost 100%, which was not achieved by conventional approaches. Further increasing the amount of PEG-SH, which made the end regions of Au NRs totally modified and the side regions of Au NRs partly modified, most of Au NRs kept the SS mode and some of them were disintegrated (Figure 3d). Immediately, when Au NRs were completely modified with PEG-SH (Figure 3e), most Au NRs were disintegrated from the SS assemblies and the SS assemblies becomes very short. Finally, the huddle Au NRs assemblies presented by adding an excessive dose of PEG-SH (Figure 3f). It is interesting that the number of EE assemblies increased gradually with increasing the PEG-SH (Figure S5, Supporting Information). In other words, the regulation of the amount of PEG-SH makes it possible for achieving the assembly transition from disorder to SS to EE.

According to the results of Au NRs assembly behaviors, the proposed assembly mechanism was presented as follows: without PEG modified on Au NRs, the assembly process of Au NRs followed the traditional water/oil interface assembly. Although the driving force from ethanol decreased the value of  $\delta$  of Au NRs and made particles move to the interface, the van der Waals forces between CTAB on Au NRs is equal for every region. Thus, most of the Au NRs were disorderly arranged after the formation of film. When the amount of PEG-SH was exactly enough for covering the ends of Au NRs completely, the assembly process was limited. When adding ethanol to

the system, the value of  $\delta$  was decreased abruptly and the Au NRs were moving to the interface. As we inferred, the synergism of CTAB and PEG made these particles band together in groups in the fastest way to reach the equilibrium. Therefore, the SS assemblies were not continued and Au NRs presented as assemblies of several Au NRs. With further increasing the amounts of PEG, the interaction became more complicated because some entanglement of PEG could also take place on sides of Au NRs. Thus, the assembly morphology was not that uniform and more EE assemblies appeared due to the high grafting density on sides of Au NRs. When Au NRs were completely covered by PEG, all CTAB were replaced by PEG-SH and the whole Au NRs was in the similar state. The powerful entanglement of PEG made them presented as clusters.

Although the macroscopic Au NRs SS assemblies can be achieved via PEG-SH and CTAB synergistically controlled interfacial assembly, there are still some uncertainties for CTAB: 1) the CTAB concentration made significant impact on assembling morphologies. CTAB were the surfactant and structural directing agent during Au NRs synthesis<sup>[52]</sup> and there was no guarantee of consistency of the amounts of CTAB after centrifugation. 2) the multiple interaction between CTAB made the spacing between Au NRs was not that uniform, which directly affected the optical properties of Au NRs assemblies.<sup>[22]</sup> Thus, introduce other chemical forces to make the directional assembly of Au NRs is of great importance. Here, another sulfhydryl molecule (1-dodecanethiol, DDT) was applied to cooperate with PEG-SH for assembling Au NRs at water/oil interface. Primarily, the ends of Au NRs were modified with PEG-SH that DDT only modified on the sides of Au NRs (Figure 4a). The hydrophobic interaction between DDT on

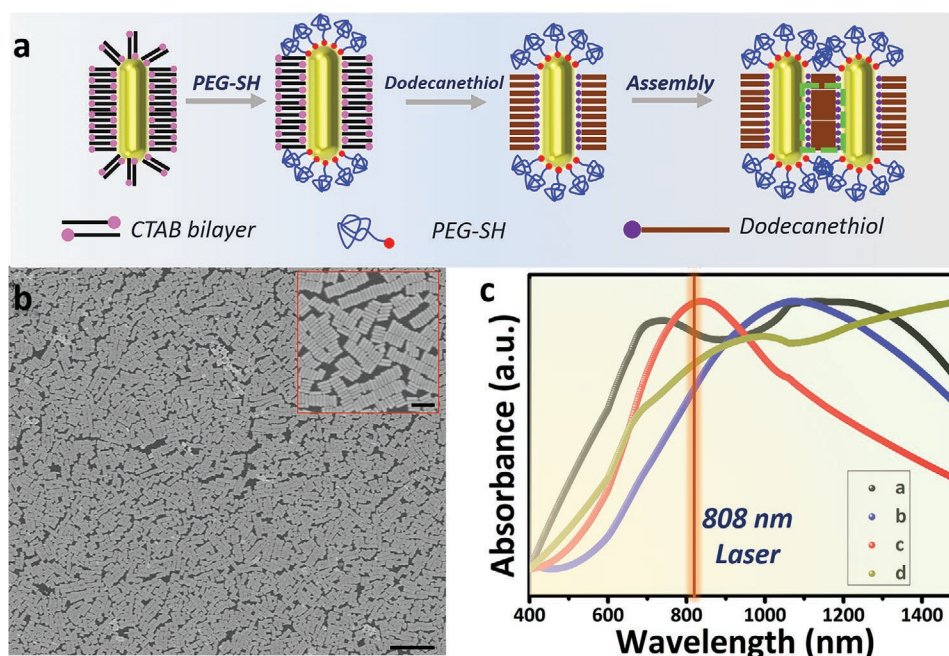


**Figure 4.** a) The schematic presentation of the modification of PEG and DDT on Au NRs and the assembly of Au NRs; b) the SEM images of the assembly of Au NRs after modified with PEG and DDT successively. The scale bar is 1  $\mu\text{m}$  (the scale bar of inset is 100 nm). c) UV-vis spectra of Au NRs assemblies obtained by anisotropic modifying Au NRs with different amount of PEG-SH and DDT; the amount of PEG-SH (10 mM) and DDT (1 mM) are as follows: a (0  $\mu\text{L}$ , 0  $\mu\text{L}$ ), b (1  $\mu\text{L}$ , 20  $\mu\text{L}$ ), c (7  $\mu\text{L}$ , 20  $\mu\text{L}$ ), d (50  $\mu\text{L}$ , 20  $\mu\text{L}$ ).

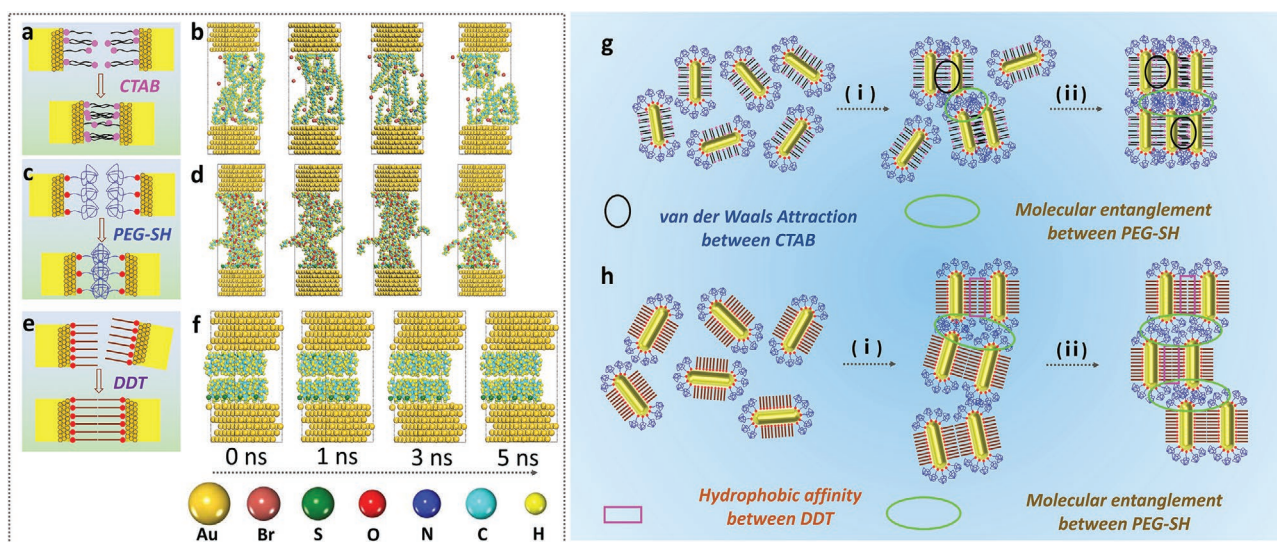


**Figure 5.** All-atom molecular dynamics simulations of three major molecules to adjust the assembly of Au NRs. a) The schematic presentation of CTAB interaction and b) the dynamics simulations of CTAB on Au NRs; c) the schematic presentation of PEG-SH interaction and d) the dynamics simulations of PEG-SH on Au NRs; e) the schematic presentation of DDT interaction and f) the dynamics simulations of DDT on Au NRs. The schematic presentation of speculated assembly procedure of g) PEG-SH/CTAB and h) PEG-SH/DDT-coated Au NRs.

sides of Au NRs and the entanglement between PEG on ends of Au NRs promoted the directional assembly of Au NRs. In previous work, DDT could convert the electrostatic repulsive force into a van der Waals interaction to motivate the orderly assembly of Au NPs.<sup>[45,65]</sup> In addition, the binding energy on Au NRs for DDT has been calculated as follows<sup>[66,67]:</sup>

$$E_{\text{int}} = \left( E_{\text{coated AuNRs}}^{\text{assembly}} - E_{\text{coated AuNRs}}^{\text{separate1}} - E_{\text{coated AuNRs}}^{\text{separate2}} \right) / S \quad (3)$$

where  $E_{\text{coated AuNRs}}^{\text{assembly}}$ ,  $E_{\text{coated AuNRs}}^{\text{separate1}}$ ,  $E_{\text{coated AuNRs}}^{\text{separate2}}$  are the total energies of assembled coated Au NRs and isolated coated Au NRs.  $S$  is the surface area.

The calculated value of DDT is around  $-4.56 \text{ J cm}^{-2}$ , which was approaching the value of CTAB ( $-4.69 \text{ J cm}^{-2}$ ). Thus, the DDT molecules satisfied the requirements to obtain the orderly Au NRs assemblies. As shown in Figure 4b, Au NRs presented as large-scaled and orderly SS assemblies with almost 100% orientational rate. In addition, the Au NRs assemblies presented distinct optical absorption by tailoring the amounts of PEG-SH and DDT (Figure 4c). It is worth noting that the SS assemblies of Au NRs showed strong absorption at 815 nm, while the disordered Au NRs assemblies showed broad absorption at 1170 nm, and the absorption of EE assemblies was beyond 1400 nm. The apparent blueshift of SS assemblies resulted from the highly ordered SS assembling that was equivalent to reducing the aspect ratio of Au NRs.

To better understand the directional assembly behavior of Au NRs, the molecular interactions on Au NRs were simulated using Forcite plus module as implemented in Materials Studio software.<sup>[68]</sup> First, CTAB interaction on two neighboring Au NRs was simulated, as shown in Figure 5a,b. In the initial state, CTAB molecules presented disorderly and irregular (0 ns). With increasing the interacting time, the staggered arrangement of CTAB molecules on adjacent two Au NRs emerged, as the position of the nitrogen atoms presented crossed (3 ns). Finally,

CTAB molecules showed total staggering (5 ns). In the light of a previous work<sup>[55]</sup> and our experimental results (Figure 2), the vdW forces between CTAB was found responsible for Au NRs interaction. However, PEG-SH molecules existed in the form of random coils and the molecules entanglement occurred gradually with increase in time (Figure 5c–e). At the equilibrium state, the strong intermolecule entanglement of PEG-SH on adjacent two Au NRs was formed (5 ns). Furthermore, the DDT molecules were disorderly distributed on Au NRs at the initial stage (Figure 5e,f). Nevertheless, the alkyl chains on the neighboring two Au NRs were gradually regularized with increase in time due to the strong hydrophobic interaction (5 ns). These simulated data were in good agreement with our experimental results and made the assembly mechanism more clear.

Furthermore, the main SS assembly process was inferred from the simulation results: 1) the ends of Au NRs were modified with PEG-SH, and sides were modified with CTAB (Figure 5g). The chain entanglement of PEG-SH on ends and the vdW forces of CTAB on sides synergistically tailored the assembly of Au NRs. It is noteworthy that these two forces were not competitive: the CTAB interaction induced the “bamboo rafts” like SS assemblies and PEG-SH entanglement made adjacent “bamboo rafts” get together. In addition, due to the hurried assembly procedure, the SS assemblies were not consecutive (Figure 2l, around dozens of Au NRs in one nano “bamboo raft”). In addition, the space between adjacent Au NRs were not uniform, due to the multiple interaction modes of neighboring CTAB molecules (Figure S3, Supporting Information). 2) The ends of Au NRs were modified with PEG-SH, and sides were modified with DDT (Figure 5h). Like CTAB, the chain entanglement of PEG-SH on ends and the hydrophobic interactions of DDT on sides synergistically promoted the assembly of Au NRs. The DDT interaction was slightly weaker than CTAB, thus the amount of Au NRs in every SS assembly was respectively less (Figure 4b). In addition, the DDT interaction

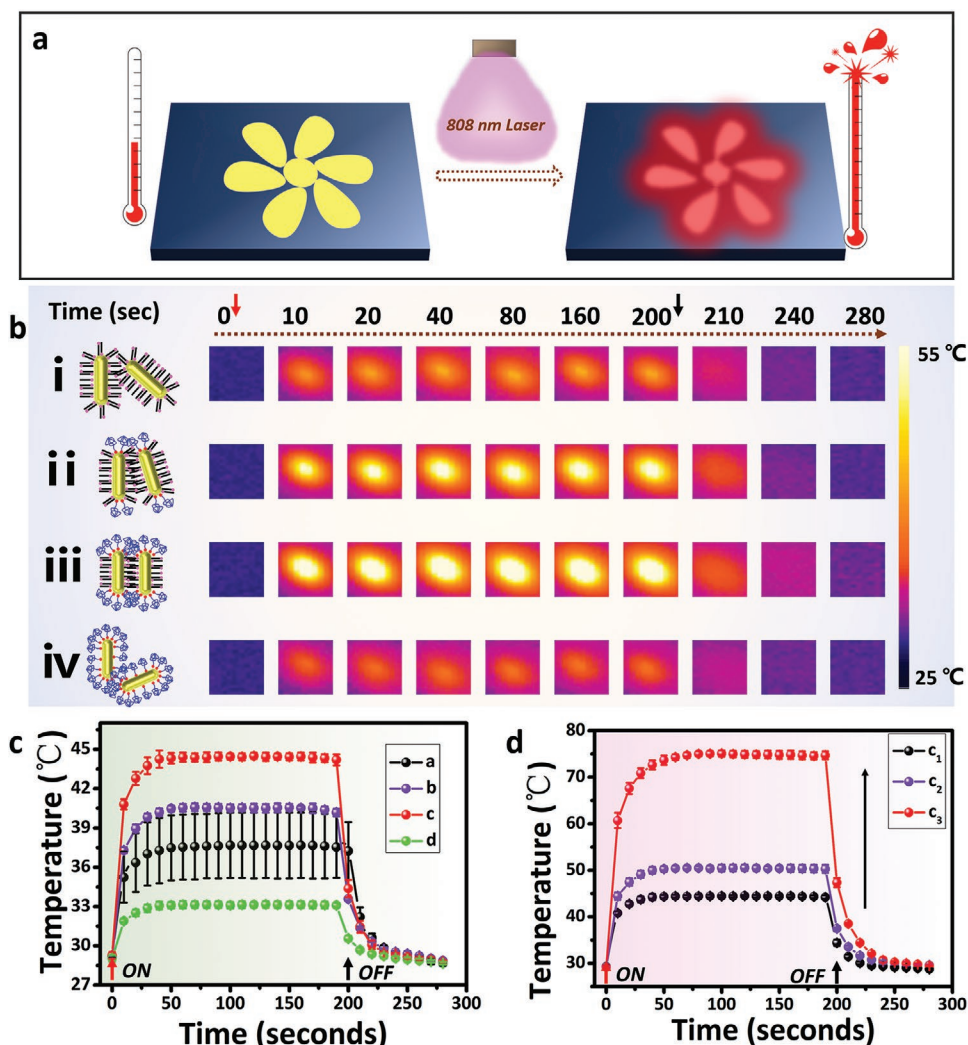


**Figure 6.** a) Schematic illustration of the photothermal conversion procedure of patterned Au NRs SS assemblies under 808 nm laser. b) Schematic illustration and the IR thermal images of different Au NRs assemblies (the PEG-SH amounts [10 mm] of (a–d) were 0, 1, 7, 50  $\mu\text{L}$ ) over time (0–300 s) under 808 nm laser of  $0.08 \text{ W cm}^{-2}$ . c) Time course of the surface temperature of different Au NRs assemblies (the PEG-SH amounts [10 mm] of (a–d) were 0, 1, 7, 50  $\mu\text{L}$ ) on PDMS over time (0–300 s) under 808 nm laser of  $0.08 \text{ W cm}^{-2}$ . d) Time course of the surface temperature of SS assemblies on PDMS over time (0–300 s) under 808 nm laser of different energy density: 0.08 ( $c_1$ ), 0.16 ( $c_2$ ), 0.4 ( $c_3$ )  $\text{W cm}^{-2}$ .

was relatively regular that the gap between Au NRs in SS assemblies was uniform and controllable (inset in Figure 4b).

The capability to convert near-infrared (NIR, 700–1100 nm) light into localized heat of Au NRs has been widely applied in various fields, especially in diagnosis and targeted therapies.<sup>[69,70]</sup> Generally, in order to achieve maximum temperature rise, many investigations were conducted to optimize the morphologies of Au NRs assemblies to match the wavelength of laser. As mentioned above, the SS assemblies obtained by interfacial assembly of asymmetric modifying Au NRs with PEG-SH and DDT showed high absorption at 815 nm, which rarely matched the 808 nm laser. In addition, the SS showed some unique characteristics compared to other similar assembling structures: 1) macroscopic and transferable; 2) stability and repeatability; 3) high orientation rate. Thus, the photothermal conversion performance of the SS assemblies were investigated (Figure 6a). In order to explore the stability of heat

conversion performance, five samples from each modified film were retrieved and measured the temperature changes after film formation (Figure S6, Supporting Information). The photothermal conversion capability of different Au NRs assemblies were estimated by measuring the surface temperature using an IR camera under 808 nm laser illumination. In order to facilitate testing, the assemblies were transferred to PDMS substrate. To compare the photothermal conversion performance of different assemblies, four typical assemblies were selected (Figure 6b). Apparently, the temperature rise (as high as 45  $^{\circ}\text{C}$ ) could be achieved under low laser energy density ( $0.08 \text{ W cm}^{-2}$ ). More importantly, the SS assemblies showed high sensitivity to laser that a temperature of 42  $^{\circ}\text{C}$  was achieved in 30 s under extremely low energy density ( $0.08 \text{ W cm}^{-2}$ ) and down to room temperature within 60 s after stop the laser (Figure 6c). In addition, higher temperature and rapid temperature rising were achieved by adjusting laser energy density (Figure 6d). When

the energy density rose to  $0.4 \text{ W cm}^{-2}$ , the temperature went up to  $50 \text{ }^\circ\text{C}$  in 10 s. In other words, the proposed SS assemblies showed higher efficiency of photothermal conversion under the energy density several times or even dozens of times lower than other similar works.<sup>[36,71,72]</sup>

However, the rise of temperature obviously weakened for other assemblies under same laser energy density (Figure 6a,b,c). In addition, the amounts of nanoparticles in a certain area will have a great impact on their photothermal conversion. However, from the perspective of photochromic devices, the stable and reusable photothermal conversion performance is as important as maximum temperature rise. Although Au NRs modified without any PEG molecules possess densely arranged parts and showed high temperature rise, they are heterogeneous and have single and multilayered structures. Apparently, the EE assemblies (Figure 6b-ii, and the curve c in Figure 6c) showed minimum temperature rise and the highest temperature only up to  $32 \text{ }^\circ\text{C}$  under  $0.08 \text{ W cm}^{-2}$ . The large redshifts of EE assemblies compared to SS ones may be responsible for the photothermal conversion difference (Figure 4c).

The optical properties of Au NPs assemblies were affected by the properties of Au NPs themselves and the spacing of particles in the assembly.<sup>[73,74]</sup> More importantly, the optical properties of Au NPs are changed after the assembly process.<sup>[75,76]</sup> The Au NPs spacing changes often result in plasma coupling changes, and the plasma resonance energy also changes after assembling.<sup>[77]</sup> Some previous work also reported that no matter what the assembly mode (SS, EE, or random arrangement) of Au NRs is, the plasma coupling after assembly increases with the decrease of Au NPs spacing and the increase of the number of Au NPs in the assembly.<sup>[78]</sup> In this work, the stronger light absorption of the SS assemblies can be attributed to the following two reasons: 1) The number of Au NRs per unit area of SS assemblies is much higher than that of EE or the random ones. As a result, the plasma coupling of SS assemblies is enhanced, further enhancing the absorption of light. 2) Plasma resonance enhancement is due to the matching of the light absorption of SS assemblies with the laser wavelength. Although the plasmon resonance properties of Au NRs after assembly are significantly different from those of Au NRs separately, the inherent nature of plasmon resonance enhancement caused by wavelength matching is unchanged. Thus, the strong absorption of Au NRs for 808 nm light is further induced due to the enhancement of plasmon resonance.

The remarkable photothermal conversion capacity of Au NRs SS assemblies is expected in thermal anticounterfeiting applications by combining with thermochromic dye. Nevertheless, the anticounterfeiting applications often require that the materials could be prepared in large area and are easy to cut.<sup>[79,80]</sup> Thus, macroscopic and a variety of patterns of SS assemblies were obtained by utilizing patterned PDMS substrates to fish up Au NRs assemblies on the surface of water (Figure S7, Supporting Information). The Au NRs SS assemblies could be easily transferred onto different patterned PDMS substrates and maintained their integrity. In addition, the rendition capability was an important evaluation parameter for anticounterfeiting applications that anticounterfeiting identification function may be used in different applications scenarios. Therefore, the rendition performance was investigated by transferring Au

NRs SS assemblies on PDMS to various substrates including paper, ceramic, plastic, and hydrophobic non-woven fabric. The Au NRs assemblies still retained their integrity that would broaden its application to various fields. Inspired by the unique feature of SS assemblies of Au NRs (such as transferrable, free-standing, macroscopic, and remarkable photothermal conversion capacity), this material is supposed to be of great values as a smart laser-responsive heat source that may be used for security protection. First, the commercial thermochromic dye were mixed with PDMS and cured together to obtain the dye layer that can be cut at will. Then different patterned SS assemblies were transferred to various substrates of demand (plastic was chosen here) followed by coating the dye layer on it (Figure 7a; Figure S8, Supporting Information).

The security mechanism of the security system we built is as follows. Upon exposure to the laser of 808 nm, SS assembly rapidly absorbs and converts it to heat and make temperature of whole security system rise. When the temperature is higher than the critical temperature of the thermochromic dye, the thermochromic dye with SS assembly at the bottom begins to discolor. As shown in Figure S9, Supporting Information, the security system can show color changes only when the ambient temperature above the critical temperature of the dye ( $40 \text{ }^\circ\text{C}$ ). Moreover, the dye color changes cannot be observed even in the presence of a laser without SS assemblies. In contrast, the dye discoloration can be observed in a very short time (1 min) after laser irradiation with SS assemblies. These results also fully demonstrated that the anticounterfeiting system we constructed has good thermal stability. When Au NRs assembled, their chemical stability was greatly improved and their chemical stability was no longer affected by temperature, ionic strength, and alkaline conditions. More importantly, even when stored for 6 months, the ink can still keep good anticounterfeiting display properties (Figure S10, Supporting Information). It is clear that the ink would maintain good stability for a long time.

The research on anticounterfeiting performance started with simple patterns such as polygons or numbers. Within 10 s, the patterns revealed clearly under a laser illumination of  $0.1 \text{ W cm}^{-2}$  (Figure 7b). In addition, the pattern disappeared rapidly in 10 min after shutting down the laser. Then, as shown in Figure 7c, some relatively complex pattern information could also be encrypted and captured. Moreover, combined SS assembly-dye layers were cut into leaf shape to enrich photothermal chromic performance (Figure 7d). After laser illumination for 10 s, the artificial leaf presented colors similar to the real leaves. Furthermore, the direct write performance was also investigated (Figure 7e) due to the point source property of laser. The combined layer of SS assemblies and dye layer served as "drawing board" and any information could be written in the area of SS assemblies. In addition, the written information could be maintained for about 10 min due to the inherent delay property of the thermochromic dye. The cyclic anticounterfeiting experiment of the composite structures were also conducted to investigate the stability and lifetime of the anticounterfeiting system. As shown in Figure S11, Supporting Information, after 10 times of repeated experiments, our security system could still maintain a good color-rendering performance. Moreover, the pattern of each display is relatively stable. It is worth noting that the proposed SS assemblies presented a simple and direct



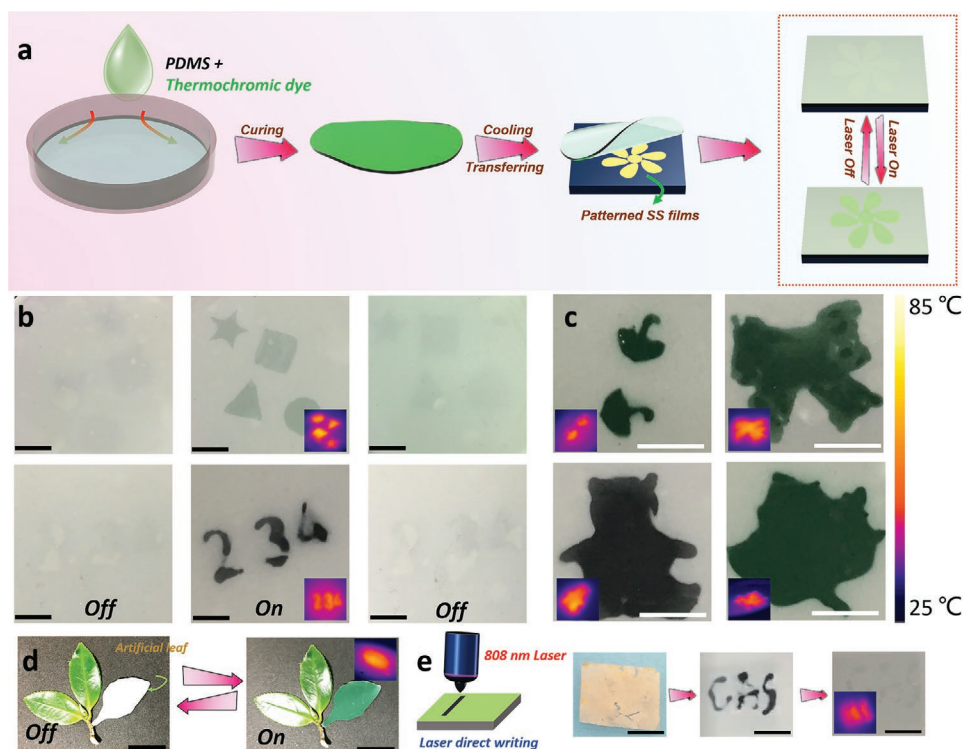


**Figure 7.** a) Schematic representation of the preparation of information encrypting composite structure. b,c) Simple anticounterfeiting displays with or without 808 nm laser ( $0.1 \text{ W cm}^{-2}$ ). d) Camouflaged “leaf” and positioned alongside real leaves without (left) and with (right) 808 nm laser ( $0.1 \text{ W cm}^{-2}$ ) exposure for 20 s. e) The laser direct writing on the composite structure of Au NRs SS assemblies and thermochromic dye. All illustrations are the corresponding IR thermal images of anticounterfeiting images. The temperature value of the anticounterfeiting displays is around  $50 \text{ }^\circ\text{C}$ . The scale bar in all images is 1 cm.

form of anticounterfeiting that required no special equipment or stimulation.<sup>[79,81]</sup> Additionally, the rapid light response endowed them sensitive discoloration performance that was of great importance for anticounterfeiting applications.<sup>[80]</sup>

### 3. Conclusion

In summary, we have successfully fabricated macroscopic and free-standing Au NRs orientational arrays via interfacial assembly. Macroscopic SS assemblies of Au NRs with almost 100% orientational rate can be obtained by precisely asymmetric modifying Au NRs with PEG/DDT. Our experimental results and simulation data showed that the van Der Waals force between DDT on sides and molecular entanglement of PEG-SH on ends of Au NRs synergistically promoted the construction of SS assemblies. In addition, the SS assemblies showed strong adsorption around 808 nm, which absolutely matched the 808 nm laser to greatly improve the photothermal conversion capability. Thus, the freestanding and macroscopic SS assemblies were applied in photothermal discoloration anticounterfeiting by combining them with thermochromic dye. Due to the unique features of SS assemblies of Au NRs (such as being transferrable, freestanding, macroscopic), various shapes and sizes of patterns could be designed for anticounterfeiting investigation and the laser direct writing could also be achieved. This study may not only provide a new strategy

to prepare orientational arrays of Au NRs, but also expand the macroscopic, freestanding, uniform, and wide-spectrum adjustable Au NRs arrays for photochromes or thermochromism applications.

### 4. Experimental Section

**General:** Tetrachloroauric acid ( $\text{HAuCl}_4 \cdot 4\text{H}_2\text{O}$ ), CTAB were purchased from Sigma-Aldrich. Silver nitrate ( $\text{AgNO}_3$ ) was purchased from Aladdin Industrial Corp. in Shanghai. Sodium borohydride, hydrogen chloride, L-ascorbic acid and 1-dodecanethiol (DDT) were obtained from Sinopharm Chemical Reagent Co., Ltd. Sodium oleate was purchased from TCI (Shanghai) Development Co., Ltd. SH-PEG-OCH<sub>3</sub> ( $M_w = 2000$ , 98%) was supplied by the J&K Chemical, Ltd. in Shanghai. All the chemicals were used without further purification.

**Synthesis of Au NRs:** The Au NRs with aspect ratio 3.5 were prepared according to Murray’s seeded growth method.<sup>[82]</sup> Prior to PEG modification, Au NRs were centrifuged twice (7500 rpm, 10 min) to remove the excess CTAB and then concentrated four times and redispersed in water.<sup>[83]</sup>

**The Exact Calculation of Asymmetric Modification of Au NRs:** The calculation process was conducted according to the previous work with little modification.<sup>[60]</sup> First, the amount of PEG for one Au NR was calculated. According to the molecular weight and structure of PEG-SH, the value of  $S_F$  of PEG-SH was confirmed as  $0.35 \text{ nm}^2$  ( $0.21 \text{ nm}^2$  for DDT).<sup>[34,35,60]</sup> The concentration of Au NRs could be calculated according to the Lambert–Beer law ( $A = \epsilon bc$ ). Therein, the value of  $b$  and  $A$  could be acquired by UV–vis spectra. According to previous study, the molar coefficient also could be obtained from according to the aspect ratio and

the LSPR peak of Au NRs solution.<sup>[33]</sup> After calculating the amount of PEG for one Au NR and the number of Au NRs, the total PEG amount could be acquired.

**Modification of Au NRs with PEG-SH:** The modification of PEG-SH was very simple. First, a certain amount of PEG-SH solid power was dissolved in deionized water with a concentration of 10 mM. Then, a certain volume of PEG-SH solution was added to the pre-prepared Au NRs solution (2 mL). The acquired solution was mixed mildly at room temperature for 24 h to make Au NRs contact with PEG-SH sufficiently. It is important to note that the amount of PEG-SH adding to Au NRs was slightly higher than the value of calculation because not all the PEG-SH in the solution adsorbed to the surface of Au NRs.

**Assembly at Water/Hexane Interface:** The assembly process was conducted according to a previous work.<sup>[22]</sup> The whole assembly process should be conducted in a stable atmosphere. Briefly, the pre-prepared Au NRs solution (2 mL) was diluted to 20 mL with water and added to the culture ware with 9 cm internal diameter. Then 10 mL hexane was slowly added dropwise on top of the water phase. These procedures should be controlled carefully to avoid part of hexane entering water phase (added rapidly or the hexane liquid drop was too big). Finally, 10 mL ethanol was injected into the water phase with a certain injecting speed (4 mm min<sup>-1</sup>). The hexane volatilized constantly and the golden film was gradually produced with continuous addition of ethanol. After the addition of ethanol and hexane volatilization were complete, the film was existed stably on the top of water phase.

**Selective Modification of Au NRs with PEG-SH and DDT Successively:** To achieve the asymmetric modification of Au NRs with PEG-SH on the ends and DDT on the sides, the PEG-SH (10 mM, 7  $\mu$ L) was preferentially added to the pre-prepared Au NRs solution (2 mL) at room temperature and mixed for 24 h. Then the mixed solution was transferred to the culture ware to conduct the assembly procedure. Different to the above process, 15  $\mu$ L DDT/hexane solution (the volume ratio of DDT to hexane was 10  $\mu$ L to 100 mL) was added to 10 mL hexane and mixed for about 1 min. Other steps were the same with the above assembly procedure. To obtain Au NRs assemblies with different adsorptions, the amount of PEG-SH was adjusted as 1, 7, and 20  $\mu$ L. The amount of DDT was same as before.

**Molecular Dynamics Simulation Studies of Self-Assembly Mechanism of Au NRs Coated with PEG-SH, CTAB, or DDT:** All simulations were performed using Forcite plus module as implemented in Materials Studio software. In order to reveal the self-assembly mechanism of Au NRs capped with PEG-SH, CTAB, or DDT, the molecular interactions and assembly processes of PEG-SH, CTAB, or DDT-coated Au (111) surface (8 PEG-SH, 14 CTAB, or 18 DDT molecules) were determined by all-atom molecular dynamics simulations. In the initial configurations, the distance between the two Au (111) surfaces exceeds 80 Å to avoid any artificial interaction between the Au NRs. In order to obtain a stable equilibrium configuration, multiple simulation approaches were carried out. Geometry minimization (less than 10 000 steps) was performed to relax these structures based on the smart minimizer method, followed by a 5 ns NVT molecular dynamic simulation at 300 K with a time step of 1 fs. Finally, a 5 ns NPT MD simulation was applied on the system to simulate the self-assembly process and obtain equilibrium structure. The interactions between atoms in the whole process were determined by COMPASS force field. The atom-based method was chosen for vdW interaction and electrostatic interaction with the cut-off distance of 12.5 Å and buffer width of 0.5 Å.

**Preparation of the Security Compositing Structure:** The patterned PDMS were synthesized by commercial embossing machine. The thermochromic dye (2 mg) and PDMS (10 g precursor and 1 g curing agent) were hybrid cured in 70 °C oven for 2 h.

**Characterization:** UV-vis absorption spectra were recorded by virtue of TU-1810 UV-vis spectrophotometer provided by Purkinje General Instrument Co., Ltd. The absorption measurement of Au NR assemblies was performed as follows: As the good light transmission of PDMS film, the cured PDMS was used as substrate to salvage Au NR assemblies. After skimming the Au NRs assemblies, the PDMS without Au NRs assemblies was used first to buckle background. Then,

the PDMS with Au NRs assemblies was pasted on the same colorimetric dish to measure the absorption spectrum of them. The morphologies of Au NRs were observed by an S-4800 (Hitachi, Japan) field emission scanning electron microscope (SEM) at an acceleration voltage of 4 kV. Transmission electron microscope (TEM) was performed on a JEOL JEM 2100 electron microscope operating at 200 kV. In all NIR-responsive experiments, a NIR laser source with a wavelength of 808 nm (BWT Beijing, K808DAHFN-15.00 W) and tunable power output of 15 W was employed.

## Supporting Information

Supporting Information is available from the Wiley Online Library or from the author.

## Acknowledgements

The authors gratefully acknowledge the National Natural Science Foundation of China (grant no. 51873222), Key Research Program of Frontier Sciences, Chinese Academy of Sciences (QYZDB-SSW-SLH036), and the Fujian Province-Chinese Academy of Sciences STS project (2017T31010024).

## Conflict of Interest

The authors declare no conflict of interest.

## Keywords

anticounterfeiting, gold nanorods, interfacial assembly, macroscopic assembly, nanorod arrays, photothermal conversion

Received: December 12, 2019

Revised: June 6, 2020

Published online:

- [1] W. Wei, F. Bai, H. Fan, *Angew. Chem., Int. Ed.* **2019**, *58*, 11956.
- [2] K. Thorkelsson, P. Bai, T. Xu, *Nano Today* **2015**, *10*, 48.
- [3] J. Xue, F. Chen, M. Bai, X. Yu, J. Wei, P. Huang, Y. Zhao, *ChemNanoMat* **2017**, *3*, 725.
- [4] S. Zhang, C. I. Pelligra, X. Feng, C. O. Osuji, *Adv. Mater.* **2018**, *30*, 1705794.
- [5] L. Chen, Y. Huang, L. Song, W. Yin, L. Hou, X. Liu, T. Chen, *ACS Appl. Mater. Interfaces* **2019**, *11*, 36259.
- [6] P. Zheng, S. Kasani, N. Wu, *Nanoscale Horiz.* **2019**, *4*, 516.
- [7] M. Sun, L. Xu, W. Ma, X. Wu, H. Kuang, L. Wang, C. Xu, *Adv. Mater.* **2016**, *28*, 898.
- [8] J. Chen, Y. Huang, P. Kannan, L. Zhang, Z. Lin, J. Zhang, T. Chen, L. Guo, *Anal. Chem.* **2016**, *88*, 2149.
- [9] Z. Zhao, Z. Zhou, G. Zhang, R. C. Chiechi, *Nanoscale Horiz.* **2016**, *1*, 473.
- [10] J. V. M. Grzelczak, E. M. Furst, L. M. Liz-Marzán, *ACS Nano* **2010**, *4*, 3591.
- [11] G. Jiang, M. J. A. Hore, S. Gam, R. J. Composto, *ACS Nano* **2012**, *6*, 1578.
- [12] Y. Ye, Z. Liu, W. Zhang, X. Cheng, S. He, *Adv. Mater. Interfaces* **2019**, *6*, 1900975.
- [13] S. T. Jones, R. W. Taylor, R. Esteban, E. K. Abo-Hamed, P. H. Bomans, N. A. Sommerdijk, J. Aizpurua, J. J. Baumberg, O. A. Scherman, *Small* **2014**, *10*, 4298.

- [14] G. Cheng, D. Xu, Z. Lu, K. Liu, *ACS Nano* **2019**, *13*, 1479.
- [15] L. Chen, B. Su, L. Jiang, *Chem. Soc. Rev.* **2019**, *48*, 8.
- [16] Z. Nie, D. Fava, E. Kumacheva, S. Zou, G. C. Walker, M. Rubinstein, *Nat. Mater.* **2007**, *6*, 609.
- [17] Z. Sun, W. Ni, Z. Yang, X. Kou, L. Li, J. Wang, *Small* **2008**, *4*, 1287.
- [18] L. Song, Y. Huang, Z. Nie, T. Chen, *Nanoscale* **2020**, *12*, 7433.
- [19] Z. Mei, L. Tang, *Anal. Chem.* **2017**, *89*, 633.
- [20] L. Hu, M. Chen, X. Fang, L. Wu, *Chem. Soc. Rev.* **2012**, *41*, 1350.
- [21] Y. Rong, L. Song, P. Si, L. Zhang, X. Lu, J. Zhang, Z. Nie, Y. Huang, T. Chen, *Langmuir* **2017**, *33*, 13867.
- [22] Y. Shin, J. Song, D. Kim, T. Kang, *Adv. Mater.* **2015**, *27*, 4344.
- [23] Z. Mao, H. Xu, D. Wang, *Adv. Funct. Mater.* **2010**, *20*, 1053.
- [24] L. Zhang, F. Liu, Y. Zou, X. Hu, S. Huang, Y. Xu, L. Zhang, Q. Dong, Z. Liu, L. Chen, Z. Chen, W. Tan, *Anal. Chem.* **2018**, *90*, 11183.
- [25] H. Lin, L. Song, Y. Huang, Q. Cheng, Y. Yang, Z. Guo, F. Su, T. Chen, *ACS Appl. Mater. Interfaces* **2020**, *12*, 11296.
- [26] Y. Shen, X. Cheng, G. Li, Q. Zhu, Z. Chi, J. Wang, C. Jin, *Nanoscale Horiz.* **2016**, *1*, 290.
- [27] X. Lu, Y. Huang, B. Liu, L. Zhang, L. Song, J. Zhang, A. Zhang, T. Chen, *Chem. Mater.* **2018**, *30*, 1989.
- [28] B. Liu, X. Lu, Z. Qiao, L. Song, Q. Cheng, J. Zhang, A. Zhang, Y. Huang, T. Chen, *Langmuir* **2018**, *34*, 13047.
- [29] P. Kumar, S. Singh, B. K. Gupta, *Nanoscale* **2016**, *8*, 14297.
- [30] C. Kuemin, L. Nowack, L. Bozano, N. D. Spencer, H. Wolf, *Adv. Funct. Mater.* **2012**, *22*, 702.
- [31] Y. Takenaka, Y. Matsuzawa, T. Ohzono, *Chem. Lett.* **2019**, *48*, 1292.
- [32] X. Liu, G. Qi, A. M. G. Park, A. Rodriguez-Gonzalez, A. Enotiadis, W. Pan, V. Kosma, G. D. Fuchs, B. J. Kirby, E. P. Giannelis, *Small* **2019**, *15*, 1901666.
- [33] C. J. Orendorff, C. J. Murphy, *J. Phys. Chem. B* **2006**, *110*, 3990.
- [34] T. Chen, C. Du, L. H. Tan, Z. Shen, H. Chen, *Nanoscale* **2011**, *3*, 1575.
- [35] P. Wuelfing, S. M. Gross, D. T. Miles, R. W. Murray, *J. Am. Chem. Soc.* **1998**, *120*, 12696.
- [36] W. Chen, J. Guo, Q. Zhao, P. Gopalan, A. T. Fafarman, A. Keller, M. Zhang, Y. Wu, C. B. Murray, C. R. Kagan, *ACS Nano* **2019**, *13*, 7493.
- [37] X. Ye, C. Zheng, J. Chen, Y. Gao, C. B. Murray, *Nano Lett.* **2013**, *13*, 765.
- [38] Z. L. W. B. Nikoobakht, M. A. El-Sayed, *J. Phys. Chem. B* **2000**, *104*, 8635.
- [39] T. K. Sau, C. J. Murphy, *Langmuir* **2005**, *21*, 2923.
- [40] S. F. Tan, S. Raj, G. Bisht, H. V. Annadata, C. A. Nijhuis, P. Kral, U. Mirsaidov, *Adv. Mater.* **2018**, *30*, 1707077.
- [41] S. Yun, Y.-K. Park, S. K. Kim, S. Park, *Anal. Chem.* **2007**, *79*, 8584.
- [42] G. Lu, H. Li, H. Zhang, *Small* **2012**, *8*, 1336.
- [43] M. Wang, Z. Zhang, J. He, *Langmuir* **2015**, *31*, 12911.
- [44] G. Yang, L. Hu, T. D. Keiper, P. Xiong, D. T. Hallinan, Jr., *Langmuir* **2016**, *32*, 4022.
- [45] Y.-K. Park, S. Park, *Chem. Mater.* **2008**, *20*, 2388.
- [46] F. Reincke, S. G. Hickey, W. K. Kegel, D. Vanmaekelbergh, *Angew. Chem., Int. Ed.* **2004**, *43*, 458.
- [47] N. Saleh, T. Phenrat, K. Sirk, B. Dufour, J. Ok, T. Sarbu, K. Matyjaszewski, R. D. Tilton, G. V. Lowry, *Nano Lett.* **2005**, *5*, 2489.
- [48] F. Reincke, W. K. Kegel, H. Zhang, M. Nolte, D. Wang, D. Vanmaekelbergh, H. Möhwald, *Phys. Chem. Chem. Phys.* **2006**, *8*, 3828.
- [49] E. W. Edwards, M. Chanana, D. Wang, H. Mohwald, *Angew. Chem., Int. Ed.* **2008**, *47*, 320.
- [50] H. Duan, D. Wang, D. G. Kurth, H. Mohwald, *Angew. Chem., Int. Ed.* **2004**, *43*, 5639.
- [51] L. Cheng, A. Liu, S. Peng, H. Duan, *ACS Nano* **2010**, *4*, 6098.
- [52] H. Chen, L. Shao, Q. Lia, J. Wang, *Chem. Soc. Rev.* **2013**, *42*, 2679.
- [53] H. Moustouai, D. Movia, N. Dupont, N. Bouchemal, S. Casale, N. Djaker, P. Savarin, A. Prina-Mello, M. L. de la Chapelle, J. Spadavecchia, *ACS Appl. Mater. Interfaces* **2016**, *8*, 19946.
- [54] N. R. Jana, L. A. Gearheart, S. O. Obare, C. J. Johnson, K. J. Edler, S. Mann, C. J. Murphy, *J. Mater. Chem.* **2002**, *12*, 2909.
- [55] K. J. Bishop, C. E. Wilmer, S. Soh, B. A. Grzybowski, *Small* **2009**, *5*, 1600.
- [56] Y. Zhu, H. Kuang, L. Xu, W. Ma, C. Peng, Y. Hua, L. Wang, C. Xu, *J. Mater. Chem.* **2012**, *22*, 2387.
- [57] A. Lukach, K. Liu, H. Therien-Aubin, E. Kumacheva, *J. Am. Chem. Soc.* **2012**, *134*, 18853.
- [58] F. C. Leung, S. Y. Leung, C. Y. Chung, V. W. Yam, *J. Am. Chem. Soc.* **2016**, *138*, 2989.
- [59] S. F. Tan, U. Anand, U. Mirsaidov, *ACS Nano* **2017**, *11*, 1633.
- [60] L. Zhong, X. Zhou, S. Bao, Y. Shi, Y. Wang, S. Hong, Y. Huang, X. Wang, Z. Xie, Q. Zhang, *J. Mater. Chem.* **2011**, *21*, 14448.
- [61] Y. Wang, Y. F. Li, J. Wang, Y. Sang, C. Z. Huang, *Chem. Commun.* **2010**, *46*, 1332.
- [62] K. K. Caswell, J. N. Wilson, U. H. F. Bunz, C. J. Murphy, *J. Am. Chem. Soc.* **2003**, *125*, 13914.
- [63] C. J. Murphy, T. K. Sau, A. M. Gole, C. J. Orendorff, J. Gao, L. Gou, S. E. Hunyadi, T. Li, *J. Phys. Chem. B* **2005**, *109*, 13857.
- [64] X. Qian, X. H. Peng, D. O. Ansari, Q. Yin-Goen, G. Z. Chen, D. M. Shin, L. Yang, A. N. Young, M. D. Wang, S. Nie, *Nat. Biotechnol.* **2008**, *26*, 83.
- [65] Y.-K. Park, S.-H. Yoo, S. Park, *Langmuir* **2007**, *23*, 10505.
- [66] H. Sun, P. Ren, J. R. Fried, *Comput. Theor. Polym. Sci.* **1998**, *8*, 229.
- [67] H. Sun, *J. Phys. Chem. B* **1998**, *102*, 7338.
- [68] BIOVIA Materials Studio 7.0, <http://accelrys.com/products/materials-studio/>.
- [69] F. Zhao, Y. Zhao, Y. Liu, X. Chang, C. Chen, Y. Zhao, *Small* **2011**, *7*, 1322.
- [70] Y. Wang, K. C. L. Black, H. Luehmann, W. Li, Y. Zhang, X. Cai, D. Wan, S.-Y. Liu, M. Li, P. Kim, Z.-Y. Li, L. V. Wang, Y. Liu, Y. Xia, *ACS Nano* **2013**, *7*, 2068.
- [71] Y. Yang, X. Yang, L. Fu, M. Zou, A. Cao, Y. Du, Q. Yuan, C.-H. Yan, *ACS Energy Lett.* **2018**, *3*, 1165.
- [72] Y. Liu, S. Yu, R. Feng, A. Bernard, Y. Liu, Y. Zhang, H. Duan, W. Shang, P. Tao, C. Song, T. Deng, *Adv. Mater.* **2015**, *27*, 2768.
- [73] W. Chen, M. Tymchenko, P. Gopalan, X. Ye, Y. Wu, M. Zhang, C. B. Murray, A. Alu, C. R. Kagan, *Nano Lett.* **2015**, *15*, 5254.
- [74] A. T. Fafarman, S. H. Hong, H. Caglayan, X. Ye, B. T. Diroll, T. Paik, N. Engheta, C. B. Murray, C. R. Kagan, *Nano Lett.* **2013**, *13*, 350.
- [75] C. A. Mirkin, R. L. Letsinger, R. C. Mucic, J. J. Storhoff, *Nature* **1996**, *382*, 607.
- [76] L. M. Liz-Marzán, *Langmuir* **2006**, *22*, 32.
- [77] K.-H. Su, Q.-H. Wei, X. Zhang, J. J. Mock, D. R. Smith, S. Schultz, *Nano Lett.* **2003**, *3*, 1087.
- [78] P. K. Jain, S. Eustis, M. A. El-Sayed, *J. Phys. Chem. B* **2006**, *110*, 18243.
- [79] S. Tao, S. Lu, Y. Geng, S. Zhu, S. A. T. Redfern, Y. Song, T. Feng, W. Xu, B. Yang, *Angew. Chem., Int. Ed.* **2018**, *57*, 2393.
- [80] K. Jiang, Y. Wang, C. Cai, H. Lin, *Adv. Mater.* **2018**, *30*, 1800783.
- [81] M. Gu, Q. Zhang, S. Lamon, *Nat. Rev. Mater.* **2016**, *1*.
- [82] X. Ye, C. Zheng, J. Chen, Y. Gao, C. B. Murray, *Nano Lett.* **2013**, *13*, 765.
- [83] L. Dai, L. Song, Y. Huang, L. Zhang, X. Lu, J. Zhang, T. Chen, *Langmuir* **2017**, *33*, 5378.